Peer-reviewed version available at Sensors 2017, 17, 2768; doi:10.3390/s17122768

Article

Embedded Conjugated Polymer Sensor Arrays for Load Transmission Measurement in Orthopaedic Implants

Carolina Micolini[1], Frederick Benjamin Holness[1], James A. Johnson[2] and Aaron David Price[1]

[1] Organic Mechatronics and Smart Materials Laboratory Mechanical and Materials Engineering, University of Western Ontario, London, ON N6A 5B9, Canada; cmicolin@uwo.ca (C.M.); fholness@uwo.ca (F.H.)
[2] Lawson Health Research Institute, University of Western Ontario, London, ON N6C 2R5, Canada; jim.johnson@sjhc.london.on.ca
* Correspondence: aaron.price@uwo.ca; Tel.: +1-519-661-2111, ext. 86420

Abstract: Load transfer through orthopaedic joint implants is poorly understood. The longer-term outcomes of these implants are just starting to be studied, making it imperative to monitor contact loads across the entire joint implant interface to elucidate the force transmission and distribution mechanisms exhibited by these implants in service. This study proposes and demonstrates the design, implementation, and characterization of a 3D-printed smart polymer sensor array using conductive polyaniline (PANI) structures embedded within a polymeric parent phase. The piezoresistive characteristics of PANI were studied to characterize the sensing behaviours inherent to these embedded pressure sensor arrays. PANI's stable response to a continuous load, its stability throughout loading and unloading cycles, and its repeatable and linear response to incremental loading cycles together with the accuracy of these measurements were investigated. It is demonstrated that this specially developed multi-material additive manufacturing process for polyaniline is an attractive approach for the fabrication of implant components having embedded smart-polymer sensors for the measurement and analysis of joint loads in orthopaedic implants.

Keywords: intrinsically conductive polymers; piezoresistance; polyaniline; sensing array; orthopaedic joint implants; reverse total shoulder arthroplasty; conjugated polymers

1. Introduction

Polyaniline (PANI) is an established conductive organic polymer that has been thoroughly investigated. In several studies, it has been established that PANI has a negative gauge factor (GF) [1,2]. The gauge factor is the ratio of relative change in electrical resistance R, as a function of the mechanical strain, and it characterizes the sensitivity of piezoresistive materials [3]. This feature, in addition to its low-cost, ease of synthesis and good environmental stability, suggests that PANI is a plausible candidate for the fabrication of piezoresistive sensors [4–8]. However, the use of this polymer for the manufacture of sensors based on its piezoresistive properties deserves further investigation [9].

An exciting application of the aforementioned technology is the use of embedded transducers within orthopaedic implants, as load transfer through theses devices is poorly understood. One example is the reconstruction of the shoulder which is an operation becoming very popular and in high demand with the "baby-boomer" population. Total reverse shoulder arthroplasty (RSTA) is in particular a relatively new procedure that has shown promising short-term results for the treatment of glenohumeral arthritis and massive rotator cuff tears, and as a salvage procedure following failure of unconstrained anatomical total shoulder arthroplasty [10–12]. The Glenohumeral joint, is a ball and socket joint, formed between the articulation of the rounded humeral head and the rounded socket (glenoid fossa) of the scapula. It is a muscle-dependent joint as it lacks strong ligaments. In a reverse total shoulder replacement the articulation is reversed: the articulating head, a spherical cobalt chromium glenoid component, is fixed to the scapula and the socket, a convex Ultra-High Molecular Weight Polyethylene (UHMWPE) humeral component, is fixed to the upper end of the humerus. The

reverse shoulder replacement is relatively new, therefore the longer-term outcomes of this implant are just starting to be understood. It is known that failure rates can be as four times higher than with the anatomical shoulder replacements, but it presents great benefits for cases in which the latter cannot be used [13].

The aim of this study is to implement our design of a 3D-printed polymer sensor, using conductive PANI structures, as an embedded smart-polymer sensor into the humeral component of the prosthesis used in Reverse Total Shoulder Arthroplasty (RTSA). The motivation for this design is to elucidate the stress distribution on the humeral cup and identify possible critical wear patterns in the humeral component. Previous efforts to measure contact points have been restricted mostly to strain gauges to measure contact loads at a discrete point of the implant's surface. It is imperative to monitor contact loads across the entire area, wherein the measurement of loads at discrete points on (or within) the implant is of particular interest since certain joint forces measured using the aforementioned techniques do not seem significant in terms of body weight, yet if these loads are concentrated on a single point they can result in wear and plastic deformation of the UHMWPE component [14]. This measuring technique will result as an improved understanding of force transmission mechanisms encountered by these implants in service and could lead to better designs, and ultimately, a reduction in notching and longer implant lifespans [15–19]. Polymers enable an approximation of the characteristics of the implant without a modification to the implant's internal structure, which leads to a more accurate measurement of the internal loads. This paper presents the characterization of polyaniline as a sensing element for internal forces in joint implants as conceptualized in Figure 1. In this regard, a 3D-printed flat sensor was created using in a 3×3 array of PANI rectangular prisms embedded in a flexible polymeric substrate.

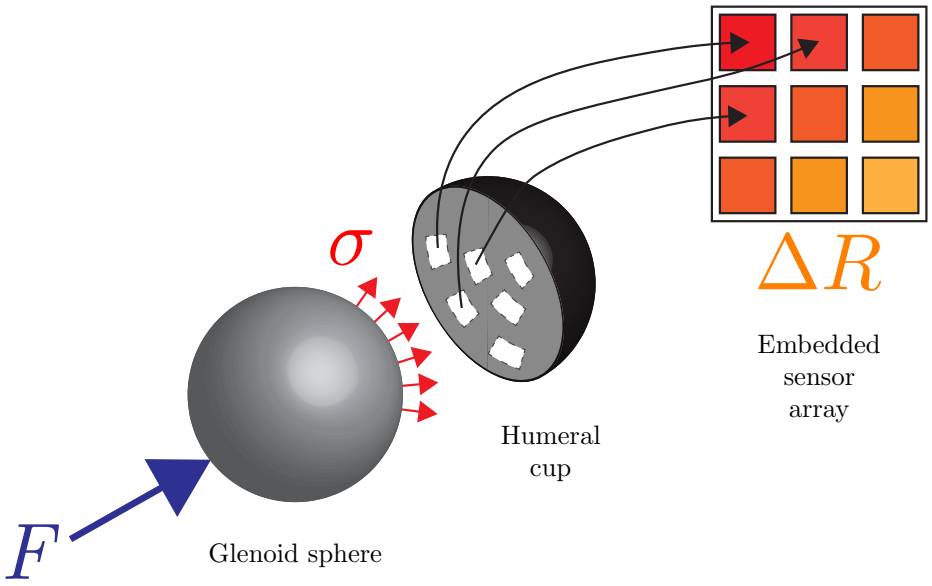

Figure 1. Conceptual representation of an orthopaedic implant with an embedded smart polymer sensor network.

2. Materials and Methods

2.1. Design and fabrication

The piezoresistive property of PANI was harnessed as a pressure sensor for the 3D-printed part. The model of the sensor was created using SolidWorks 2016 R2016a (Dassault systemes, France) in a 3×3 array of polyaniline rectangular prisms embedded in a flexible polymeric substrate. This pattern

Peer-reviewed version available at Sensors 2017, 17, 2768; doi:10.3390/s17122768

was created to demonstrate that it is possible to distinguish between different pressures in various areas, monitoring across the whole surface. The model of the flexible polymeric substrate was 3D printed using thermoplastic elastomer filament in the shore hardness 95A (Ninjatek, USA) with infill configured to 15% and PANI doped by the use of dodecyl benzene sulfonic acid (DBSA) prepared according to the protocols described by Holness *et al.* [20]. To this end, a specialized multi-material 3D printing technique has been developed at Western's Organic Mechatronics and Smart Materials Laboratory for direct-ink writing processes using a modified fused filament fabrication delta robot equipped with an integrated polymer paste extruder, which has been discussed in detail elsewhere [20]. The flexible polymeric substrate includes a removable base where the PANI is injected to affix the part onto the build plate during printing. The dimensions of the sensor were 30 mm $\times$ 30 mm $\times$ 2.5 mm. This dimension represents the approximate area of the humeral cup of an RTSA. The size of each polyaniline rectangular prism was 3.5 mm $\times$ 3.5 mm $\times$ 2.5 mm, and the distance between the centers of each element was 9 mm. The unwired-sensor was weighted before the thermal treatment of 165 °C for 5 min on a covered hot plate [9]. After each PANI element was treated with a thermal doping, it needed to be wired. Two methods of connection were tested to join the wires with the PANI elements: the use of conductive carbon tape and the use of silver epoxy as suggested by Blythe [21], who indicates that the uncertain contact resistances between the electrodes and the specimen can be reduced using silver paint. The accuracy by means of Root Mean Square Error (RMSE) were calculated for both methods and for all the different load levels, all the elements show an average error ranging from $RMSE_{avg,Element5} = 3.72\%$ to $RMSE_{avg,Element2} = 5.38\%$ when using silver epoxy as an element of connection between the wires and the PANI, whereas that using carbon tape, these values range from $RMSE_{avg,Element3} = 17.7\%$ to $RMSE_{avg,Element7} = 74.94\%$. These high values indicate an unstable connection between the wires and the PANI, which leads to discarding the conductive carbon tape as a method of connection for the realization of these embedded sensors, leading to choose the silver epoxy (MG Chemicals, Canada) as a means of connection.

2.2. Signal acquisition and processing

The piezoresistive effect consists of a change of the electrical resistivity of a semiconductor when mechanical strain is applied. A through-thickness sensing mode was employed to measure this change in resistance [8]. Ten voltages were measured using a 32-input compact DAQ NI 9205 (National Instruments, EUA) and an NI 9174 chassis (National Instruments, EUA). Nine of these analog inputs were used to measure the voltages from the top surface of each PANI element, and one analog input was used to measure the applied voltage (nominal value of 2 V) in the whole circuit of the two-point probe used to measure the PANI's resistance. The connection made between all the elements on the underside was connected to the ground in the circuit and in the COM channel in the DAQ NI 9205. A custom-made MATLAB (MathWorks, USA) software interface was developed to analyze the voltage signal and to calculate PANI's resistance. A voltage-divider method was used to measure the resistivity according to the following equation:

$$R = \frac{R_S}{(\frac{V_{\text{in}}}{V_R}) - 1}, \tag{1}$$

where R is the variable PANI resistance measurand, R_S is the shunt resistor of 1000 $\Omega \pm 1\%$ tolerance, in series with R, V_{in} corresponds to the input voltage to the whole circuit, including R and R_S, and V_R is the voltage drop across R. The input voltage can be defined by the user, in this case, $V_{\text{in}} = 2$ V. A filter was employed to introduce 60 Hz noise rejection while decreasing noise rejection at other frequencies. All negative resistivity was remapped to null resistivity. Equation 1 was used to measure R in each PANI element during each individual pressure load. After the range of the pressure was acquired, curve fits were applied to each of the curve data (there are nine sets of data points, one for each polyaniline element). All test were done at an applied voltage of 2 V, the voltages input value was measured by the Data Acquisition (DAQ) and used to calculate the resistance, to compensate for any variation of the power supply.

Peer-reviewed version available at Sensors 2017, 17, 2768; doi:10.3390/s17122768

2.3. Calibration apparatus

Compression tests were carried out at room temperature using a specially designed calibration apparatus as depicted in Figure 2. This apparatus consists of an air cylinder (Bimba, USA) in which the air flow was controlled by a QPV1 electronic pressure regulator (Equilibar, USA) connected to an air compressor. A flat surface of 30 mm × 30 mm was used to apply consistent pressure to the sensor. The electronic pressure regulator was driven by a NI 9263 (National Instruments, USA) on an NI 9174 chassis (National Instruments, USA). The applied load was corroborated by a LCAE 35KG load cell (Omega, USA). The pressure regulator was driven by a Data acquisition system NI 9263, and the load cell's output was measured using a DAQ 9205 on a LabVIEW interface.

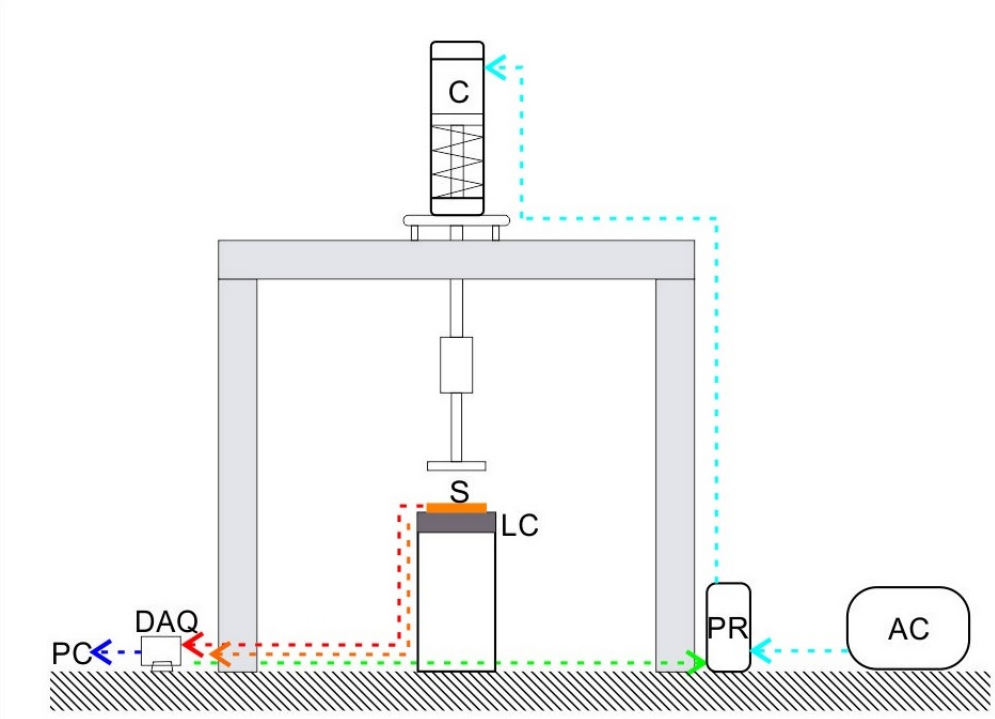

Figure 2. Calibration apparatus consisting of Air Cylinder (C), Pressure Regulator (PR), Air Compressor (AC), Data Acquisition System (DAQ), Load Cell (LC), Personal Computer (PC). A Sensor (S) is illustrated to demonstrate the placement at the time of characterization.

The software acquired the resistance measured in each PANI element during each individual pressure load. After the range of the resistance values was acquired, linear curve fits were applied to each grouping of data sets (there are nine sets of data points, one for each polyaniline element). To be used as a sensor, a graphical user interface (GUI) was created, where the software can relate the resistance measurement to the applied pressure. Afterward, the resulting data can be accessed to plot the pressure matrix when its value is unknown.

2.4. Sensor array characterization

After the sensor was printed, thermally treated, and wired, the sensor's piezoresistive characterization was undertaken, utilizing the specially designed calibration apparatus previously described, by a series of six separate tests.

2.4.1. Stability

The resistance of the elements without any applied load was measured, to then be measured under a constant load for a given period of time. The resistance of the elements was measured with no

Peer-reviewed version available at Sensors 2017, 17, 2768; doi:10.3390/s17122768

applied load for the first 160 s, in a total of 12 measurements. Afterward, a 6.78 N load was applied and the elements were left to stabilize for 35 s, after that time the first measurement of the resistance under load was taken, with a total of 41 measurements under load taken in a 1966 s period.

2.4.2. Cycle loading

Loading/unloading cycles of the elements were carried out, applying the same load in each cycle. Loaded measurements were taken using a 27.58 kPa input for the air cylinder, corresponding to a 5% input of the 551.58 kPa supplied by the air compressor of the calibration apparatus, which applies a total load of 6.78 N onto the sensor. The first measurement was taken with no applied load (R_0), the sensor was then loaded for 30 s, in order to allow the PANI stabilization at the new load level of 8.5 N [3], subsequently the loaded measurement $(R_{5\%})$ was taken. After this measurement was taken, the sensor was left unloaded for 30 s before a new cycle. This process was repeated for 40 cycles, with a total of 80 resistance measurements.

Plots were obtained by introducing the following relations:

$$Point_{0,n} = \frac{R_{0,n} - R_{0,n-1}}{R_{0,n-1}}, \tag{2}$$

$$Point_{5\%,n} = \frac{R_{5\%,n} - R_{0,n}}{R_{0,n}}, \tag{3}$$

where R_0 corresponds to the value for the unloaded-resistance measured, and $R_{5\%}$ corresponds to the value for the loaded-resistance measured.

2.4.3. Incremental loading: continuous loading

An incremental loading from 0 N up to 50.84 N, with a loading step of 3.4 N was performed. After each incremental load was applied, the elements were left to stabilize for 60 s, then the measurements were taken and the load increased again, to repeat the procedure.

The fractional change in resistance $(\Delta R/R_0)$ was calculated. ΔR is the difference between the resistance measured while the load is being applied and the resistance measured without the load over the sensor, and R_0 is resistance at no-load.

2.4.4. Incremental loading: zero breaks

An incremental loading from 20.34 N to 84.73 N, in 3.4 N steps was performed. The load was applied and the elements were left to stabilize for 60 s before measuring the loaded resistance value, after taking these measurements the load was removed and the elements were left unloaded for 60 s, before reloading the elements again with the increased load and repeating the measuring procedure up to 84.73 N.

2.4.5. Loading/unloading cycle

A Loading/Unloading cycle carrying the load from 0 N – 50.84 N, in steps of 8.5 N was performed. Then the load was decremented in steps of 8.5 N, carrying the load from 50.84 N – 0 N. During the loading cycle, the elements were subjected to loading for 60 s before taking the resistance measurement, after taking the measurement the load was increased again. During the unloading cycle, the load was decremented, and the elements were subjected to the new load for 180 s before taking the new measurement. The first measurement of the unloaded resistance was considered as 100% of the resistance value, and the rest of the resistances were calculated as a percentage of this one.

Peer-reviewed version available at Sensors 2017, 17, 2768; doi:10.3390/s17122768

2.4.6. Repeatability

Three loading/unloading cycles were performed, letting the elements to rest in between each cycle for a minimum of one hour. To have a better interpretation of the behavior of the curves, only data taken in the load cycles from 5% up to 30% are presented.

2.4.7. Accuracy

To calculate accuracy, the root mean square (RMS) of the error between the measurements taken in each one of the three loading/unloading cycles compared with respect to the average of the measurements obtained in all the cycles was calculated, using the following formula:

$$RMSE = \sqrt{\frac{1}{n}\sum_{i=1}^{n}\left(\frac{R_n - \overline{R}}{\overline{R}} \times 100\right)^2}. \quad (4)$$

3. Results

The aim of this study was to probe the capability of using a specialized multi-material 3D printing technique and the piezoresistive characteristics of PANI to manufacture embedded sensors for various applications, especially for the analysis of joint loads in orthopaedic implants. To this end, the piezoresistive characteristics of this polyaniline were analyzed.

3.1. Design and fabrication

The fabricated sensor consisting of a 3×3 array of polyaniline rectangular prisms, each one considered as an *element*, embedded in a flexible polymeric substrate, and, for simplification purposes, a schematic of the connection of one of the PANI's elements is shown in Figure 3 and Figure 4 respectively. Figure 5 illustrates the sensor's setup during all tests of piezoresistive characterization.

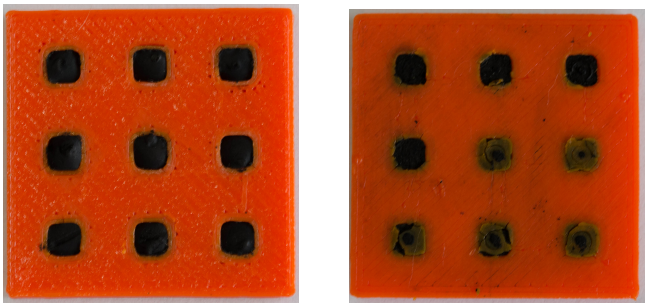

(a) (b)

Figure 3. 3D-printed sensor array without the wires **a**) Front view (**b**) Back View - bottom elements showing the base used to prevent the injected PANI to slight onto the printer's build plate.

Preprints (www.preprints.org) | NOT PEER-REVIEWED | Posted: 3 August 2017 doi:10.20944/preprints201708.0011.v1

Peer-reviewed version available at Sensors 2017, 17, 2768; doi:10.3390/s17122768

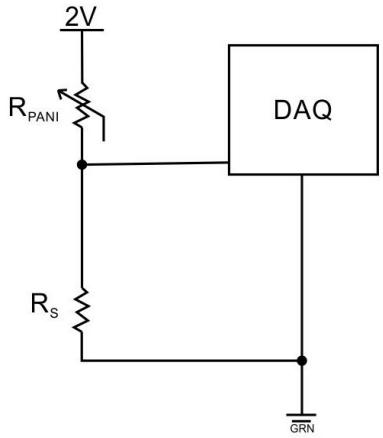

Figure 4. Schematic connection for one of the PANI's elements, consisting of PANI element (R_{PANI}), Shunt Resistor (R_S), and Data Acquisition System (DAQ) with a 2 V excitation.

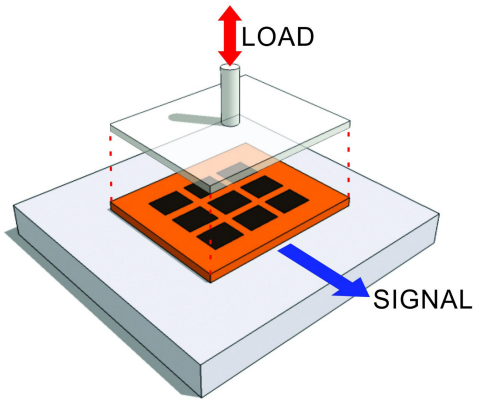

Figure 5. Scheme of the sensor's setup for piezoresistive characterization.

The unwired-sensor was weighed before the thermal treatment of 165 °C for 5 min on a covered hot plate, its initial weight was 1.8980 g. It was weighed again immediately after, and the final weight was 1.8575 g. The 0.0405 g difference is due to the loss of moisture by evaporation [22].

3.2. Sensor array characterization

3.2.1. Stability

In this test set, Element #9 was discarded due to wire connection problems. Element #1 and Element #7 have such an abrupt drop in measurement for the same reason. When the sensor was unloaded, the wires did not make a good electrical contact, which corresponds to such high resistance values. Once the load is applied, the weight generated by the air cylinder is sufficient to ensure good electrical contact. Figure 6 only shows the measurements of Elements #2, #4, #5, #6 and #8. Which shows a stable response even without load. This is done not to have the interference of the measurement of the elements that has shown bad connectivity.

Preprints (www.preprints.org) | NOT PEER-REVIEWED | Posted: 3 August 2017 doi:10.20944/preprints201708.0011.v1

Peer-reviewed version available at Sensors 2017, 17, 2768; doi:10.3390/s17122768

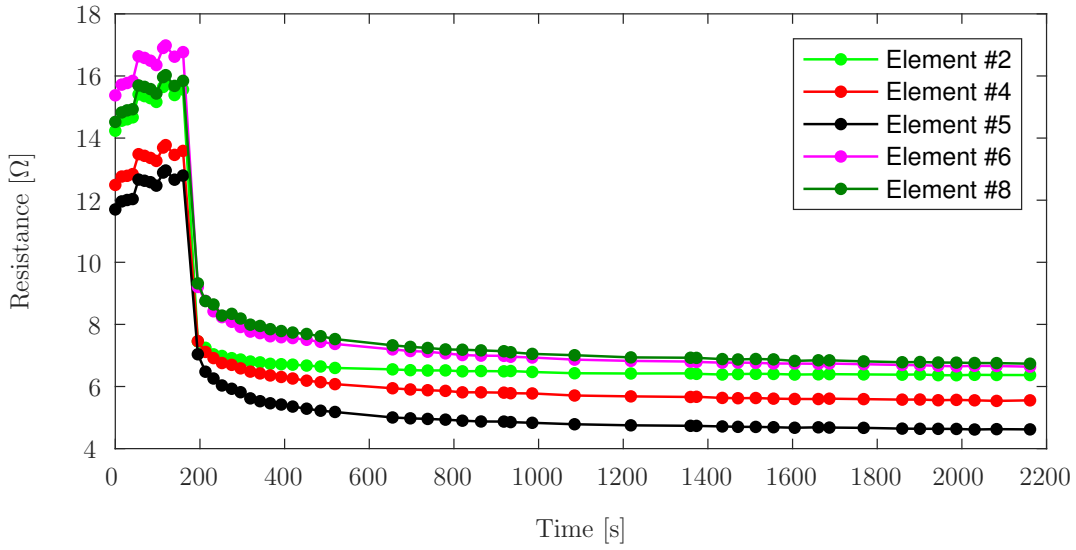

Figure 6. Change in resistance under no load and continuous load, for each PANI element.

The initial abrupt drop during the first seconds of the load can be attributed to the delay of the pneumatic piston to reach the desired load value. For all elements, the value of the resistance reaches its final stabilization around the 7th minute of continuous load application. If the first loaded measurement of resistance for each element is considered as 100% of the value for that series, the percentage dropped to a maximum of 55.7% of its initial value for Element $^{\#}1$ and a minimum of 85.45% for Element $^{\#}2$, both are the final measurements taken, with the final values of the other elements ranging in between these values.

3.2.2. Cycle loading

Two separate equations have been used to show two trends. Equation (2) shows the difference between the measurements of unloaded-resistance versus the previous unloaded-resistance.

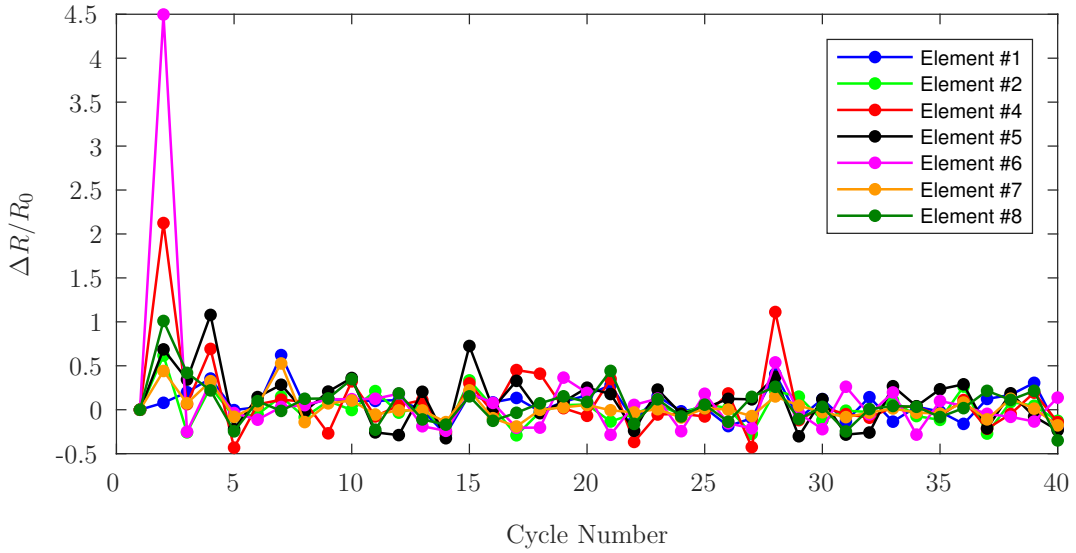

Figure 7. Fractional change in unloaded-resistance as a function of cyclic loading, for each PANI element.

Equation (3) shows the difference between the measurements of the loaded-resistance versus the value of the unloaded-resistance previous to the loading of the elements.

Preprints (www.preprints.org) | NOT PEER-REVIEWED | Posted: 3 August 2017 doi:10.20944/preprints201708.0011.v1

Peer-reviewed version available at Sensors 2017, 17, 2768; doi:10.3390/s17122768

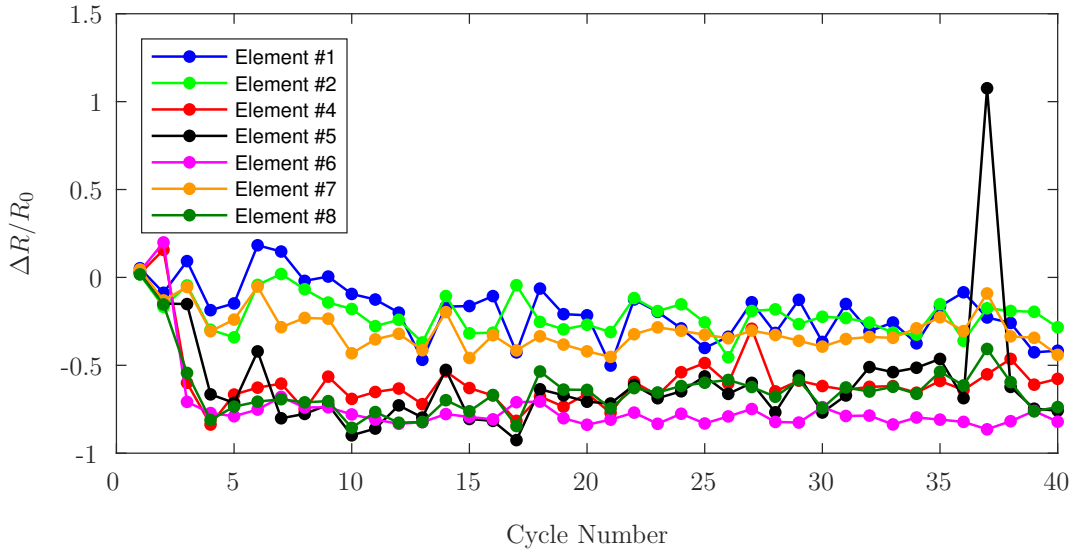

Figure 8. Fractional change in loaded-resistance as a function of cyclic loading, for each PANI element.

The disturbance observed in both graphs in cycles 37 and 38 for Element $^{\#}5$ are attributed to an overload of 170 N for this element after cycle 36.

3.2.3. Incremental continuous loading

The value of the resistance at 3.4 N of applied pressure (R_0) is considered to be 100%, all other values, at different applied pressures, are represented as a percentage of R_0. Figure 9 shows the change in resistance for each PANI element during incremental continuous loading up to 30.5 N, after that value the response of the elements tends to plateau.

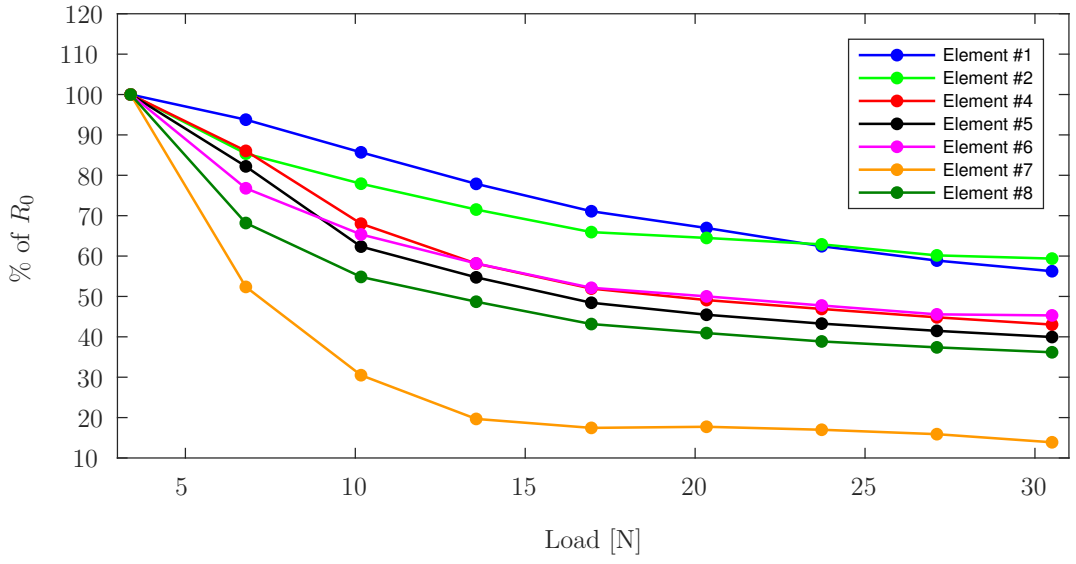

Figure 9. Change in resistance as a function of R_0 during incremental continuous loading, for each PANI element.

Alternative graph showing linear trendlines, on which it can be seen how the trend lines are similar for all elements although the values are different.

Peer-reviewed version available at Sensors 2017, 17, 2768; doi:10.3390/s17122768

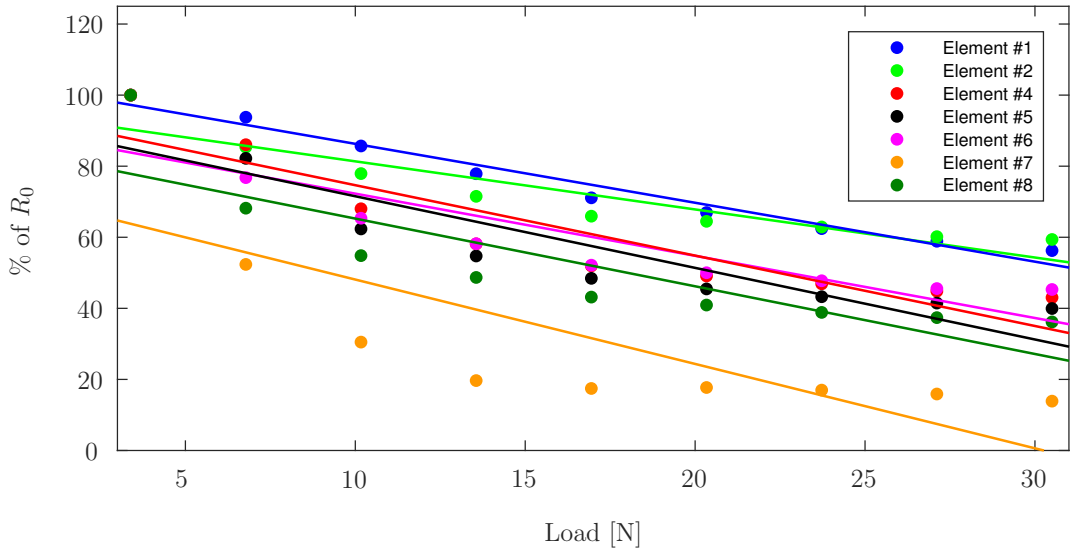

Figure 10. Linear fits for the change in resistance as a function of R_0 during incremental loading, for each PANI element.

3.2.4. Incremental loading: zero breaks

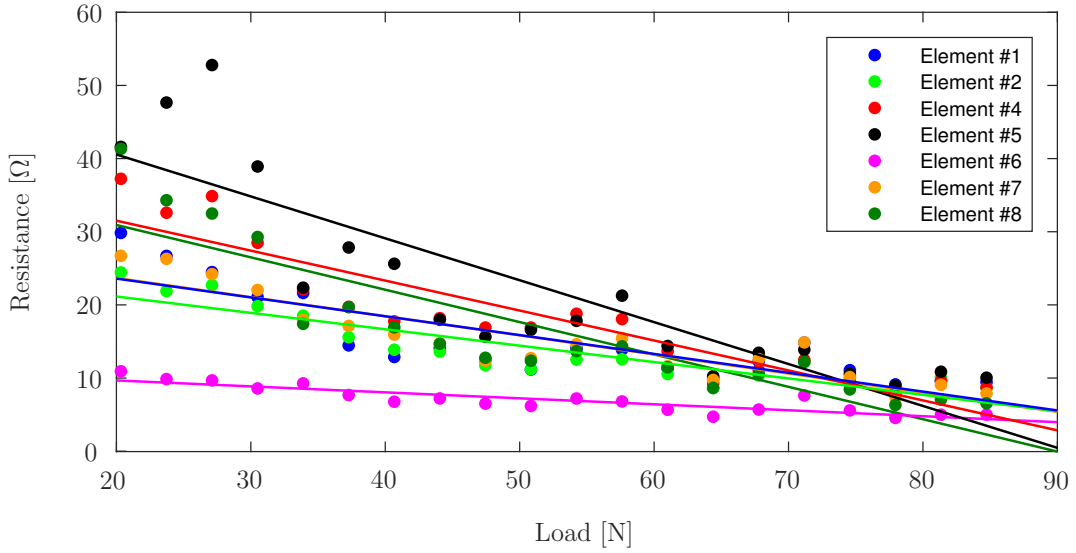

Figure 11. Linear fits for the change in resistance as a function of R_0 during incremental loading-zero breaks, for each PANI element.

Element #3 and Element #9 were left out of this graph, the former did not exhibit significant change in resistance under load, while the latter exhibited erratic behavior attributed to poor electrical connectivity.

3.2.5. Loading/unloading cycle

As all elements show similar curves, Element #4 is shown as a representative element to visualize the graph without interferences. Figure 12 shows the values measured for the relative change in resistance of Element #4 during the first loading/unloading cycle.

Preprints (www.preprints.org) | NOT PEER-REVIEWED | Posted: 3 August 2017 doi:10.20944/preprints201708.0011.v1

Peer-reviewed version available at Sensors 2017, 17, 2768; doi:10.3390/s17122768

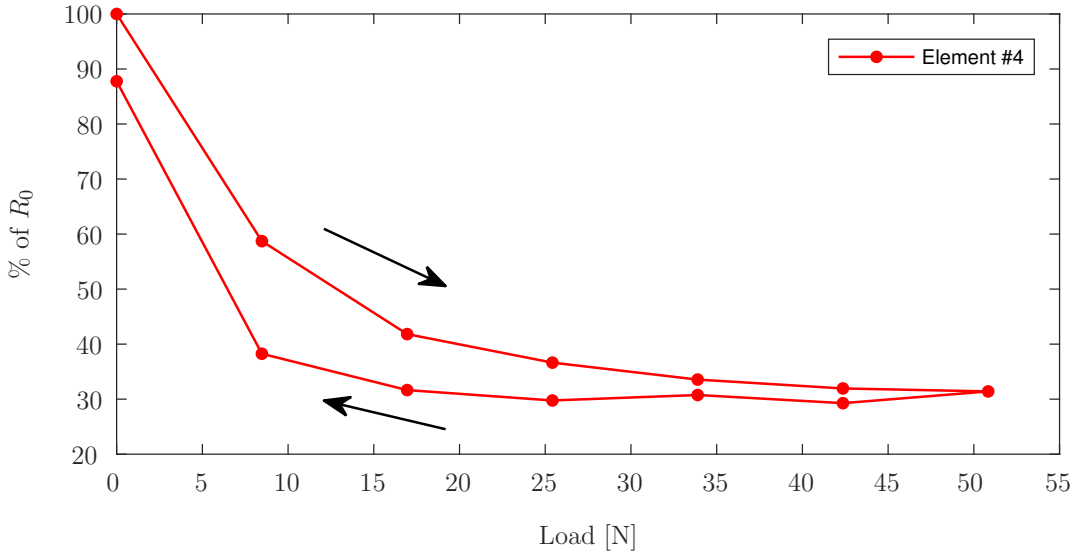

Figure 12. Relative change in resistance on Element #4 during the first loading/unloading cycle.

3.2.6. Repeatability

It can be observed in Figure 13 that the dynamics of the curve is repeated in the three cycles.

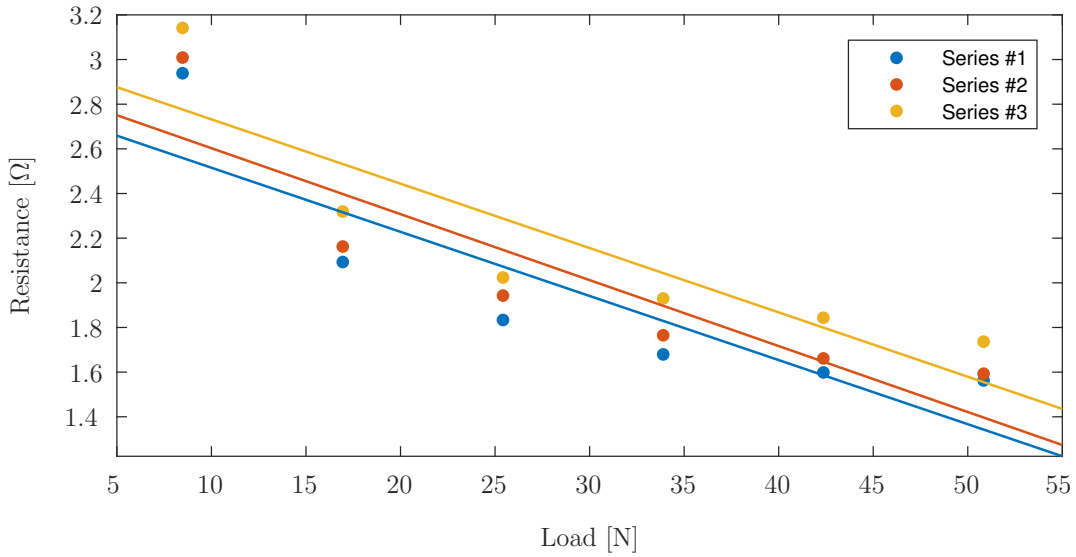

Figure 13. Change in resistance on Element #4 during the loading portion of the three repetitions of loading/unloading cycles as a function of load.

Table 1, shows the R^2 values for the linear fitting, only values for elements with good connectivity have been included.

Table 1. R^2 values for the linear fitting.

	Element #1	Element #2	Element #4	Element #5	Element #6	Element #7	Element #8
Series 1	0.81	0.85	0.76	0.79	0.78	0.80	0.81
Series 2	0.86	0.68	0.79	0.80	0.64	0.79	0.81
Series 3	0.84	0.68	0.78	0.78	0.71	0.81	0.82

3.2.7. Accuracy

The maximum value of RMSE is found for Element #6, with a value of $RMSE_{Element6,16.95N} = 7.97\%$, while the minimum value is found for Element #5, $RMSE_{Element5,8.47N} = 0.66\%$. All other elements have RMSE values in between, shown in the next table.

Table 2. Root Mean Square (RMS) of the error between the measurements taken in each one of the three loading/unloading cycles compared with respect to the average of the measurements obtained in all the cycles.

Load [N]	Element #1	Element #2	Element #4	Element #5	Element #6	Element #8
8.47	5.47%	7.19%	2.78%	0.66%	5.90%	4.88%
16.95	6.27%	5.19%	4.32%	1.99%	7.97%	5.00%
25.42	4.99%	4.49%	4.03%	2.86%	1.65%	4.41%
33.89	6.01%	5.49%	5.80%	5.24%	4.40%	3.35%
42.36	4.53%	2.71%	6.10%	6.34%	4.42%	2.98%
50.84	2.98%	7.28%	4.65%	5.21%	6.51%	4.47%

For all the different load levels, all the elements show an average error ranging from $RMSE_{avg,Element5} = 3.72\%$ to $RMSE_{avg,Element2} = 5.38\%$.

4. Discussion

In this study, a series of tests to characterize and evaluate the conductive polyaniline used for the 3D-printing technique as a potential candidate to manufacture implant components embedded with smart-polymer sensors were presented. The response of the PANI to a cyclical application of loads, its repeatable response to incremental compressive loading, the stability of its response to a continuous load, and the accuracy of these measurements, were used to corroborate the effectiveness of this material as a potential sensor. Due to the 3D printing capabilities currently available, it is not possible to ensure an identical PANI deposition for each sensing element, at the same time the different amounts of silver epoxy used for the wire connections added to the lengths of these wires are translated in different resistances values for each sensing element. After the cyclical application of loads, two separate equations have been used to show two trends. Equation (2), used for Figure 7, shows that the difference between the measurements of unloaded-resistance versus the previous unloaded-resistance tends to zero, this is consistent with the resistance returning to its pre-load value when no load is applied. This behavior is consistent with the observations reported by Barra *et al.* [22], who attribute re-organization of conduction pathways and elastic deformation of the matrix as the mechanisms for relative conductivity returning to its previous value upon unloading. Figure 8 shows the difference between the measurements of the loaded-resistance versus the value of the unloaded-resistance previous to the loading of the elements. During the cycling loading, it was observed that the measured resistance values for each element increase with each cycle in accordance with the observations made by Falletta *et al.* [7], who suggest that irregular behavior may be attributed to initial mechanical instabilities within the polymers. Both figures indicate that the fractional change in PANI's electrical resistance becomes more stable after 30 cycles. Figure 10, showing linear trend lines for the data acquired during incremental continuous loading, verify a different behavior for Elements #3 and #9 due to the faulty connection between the PANI and the wires, while the trend lines are similar for the other elements although the values are different. The same phenomenon is seen during incremental loading with zero breaks, where Element #3 does not show notables changes in resistance change measured under load or without load, and Element #9 shows erratic behavior corresponding to connectivity problems. Figure 13 shows the linear fit for the data acquired during the three cycles of piezoresistive characterization on Element #4, the resistance is plotted as a function of the applied load. Linear curve fits were applied to each set of measurements. R^2 values were obtained as high as 0.8608 for the first cycle of Element #1, with an average value of 0.7803, and the

lowest value found for Element #6 during the second loading/unloading cycle with a value of 0.6447. With the application of increasing loads, the resistivity of PANI decreased linearly. Prior studies have observed that the reduced interchain separation coupled with the enhanced interchain charge transport diminish the resistance of PANI while enduring compressive load [5,7,22]. This demonstrates that the response of the material is reliable, the limitation is the fragility of the connections between the PANI and the wires, which tend to get loose after a low number of loading cycles, but once the load was applied, the weight generated by the air cylinder is sufficient to ensure good electrical contact between the wires and the PANI elements. Others Silver Filled, Electrically Conductive Adhesives are being studied to improve the connections between the PANI elements and the wires. Future efforts will focus on the development of a 3D printed instrumented humeral cup, consistent of these PANI-based embedded sensors, as shown in Figure 1. Due to the geometry of the humeral component of these implants, it will be necessary to make modifications in the calibration apparatus in order to apply a force perpendicular to each PANI element at the time of the calibration. Furthermore, it will be necessary to adjust the custom-made MATLAB (MathWorks, USA) software interface to calibrate each PANI element individually and not altogether as is currently done for the flat sensor.

5. Conclusions

The design, fabrication, characterization, and signal acquisition and processing of a 3D-printed polymer sensor with a 3×3 conductive polyaniline structure array were presented in this paper. The piezoresistive characterization of the PANI elements embedded in the sensor, in addition to the calibration apparatus and technique, were explained. The fractional change in resistance upon continuous loading, cyclical loading and unloading, and incremental loading, as well as, the repeatability and accuracy of the loading/unloading cycles were discussed. Since the developed PANI sensor arrays present a good linear relationship between the fractional changes in resistance during incrementally applied loads, together with a stable response, this specially developed multi-material additive manufacturing process for polyaniline represents a potential candidate to manufacture implant components embedded with smart-polymer sensors. The next step is to fabricate a curved sensor, to mimic the humeral cup of a Reverse Total Shoulder Arthroplasty implant.

Acknowledgments: The authors gratefully acknowledge the financial support of NSERC Canada through Discovery Grant RGPIN-2015-05014 "Toward 3D Printing Technologies for the Fabrication of Nanoscale Actuator Arrays." Carolina Micolini would like to thank the Organization of American States for its financial support through the "OAS Regular Program for Academic Scholarships (Graduate)."

Author Contributions: C.M. conceived, designed and performed the experiments, analyzed the data, and wrote the paper; B.H. prepared the PANI, supervised the 3-D printing, and helped prepare the figures; J.J. critically reviewed the study; and A.P. closely supervised and reviewed the study.

Conflicts of Interest: The authors declare no conflict of interest.

References

1. Lillemose, M.; Spieser, M.; Christiansen, N.O.; Christensen, A.; Boisen, A. Intrinsically conductive polymer thin film piezoresistors. *Microelectronic Engineering* **2008**, *85*, 969–971.
2. Pereira, J.N.; Vieira, P.; Ferreira, A.; Paleo, A.J.; Rocha, J.G.; Lanceros-Méndez, S. Piezoresistive effect in spin-coated polyaniline thin films. *Journal of Polymer Research* **2012**, *19*, 9815.
3. Della Pina, C.; Zappa, E.; Busca, G.; Sironi, A.; Falletta, E. Electromechanical properties of polyanilines prepared by two different approaches and their applicability in force measurements. *Sensors and Actuators, B: Chemical* **2014**, *201*, 395–401.
4. Adams, P.N.; Laughlin, P.J.; Monkman, A.P.; Bernhoeft, N. A further step towards stable organic metals. Oriented films of polyaniline with high electrical conductivity and anisotropy. *Solid State Communications* **1994**, *91*, 875–878.
5. Bao, Z.X.; Colon, F.; Pinto, N.J.; Liu, C.X. Pressure dependence of the resistance in polyaniline and poly(o-toluidine) at room temperature. *Synthetic Metals* **1998**, *94*, 211–213.

6. Razak, S.I.A.; Dahli, F.N.; Wahab, I.F.; Abdul Kadir, M.R.; Muhamad, I.I.; Yusof, A.H.M.; Adeli, H. A Conductive polylactic acid/polyaniline porous scaffold via freeze extraction for potential biomedical applications. *Soft Materials* **2016**, *14*, 78–86.
7. Falletta, E.; Costa, P.; Della Pina, C.; Lanceros-Mendez, S. Development of high sensitive polyaniline based piezoresistive films by conventional and green chemistry approaches. *Sensors and Actuators, A: Physical* **2014**, *220*, 13–21.
8. Kang, J.H.; Park, C.; Scholl, J.A.; Brazin, A.H.; Holloway, N.M.; High, J.W.; Lowther, S.E.; Harrison, J.S. Piezoresistive Characteristics of Single Wall Carbon Nanotube/Polyimide Nanocomposites. *Journal of Polymer Science Part B: Polymer physics* **2009**, *47*, 994–1003.
9. Del Castillo-Castro, T.; Castillo-Ortega, M.M.; Encinas, J.C.; Herrera Franco, P.J.; Carrillo-Escalante, H.J. Piezo-resistance effect in composite based on cross-linked polydimethylsiloxane and polyaniline: Potential pressure sensor application. *Journal of Materials Science* **2012**, *47*, 1794–1802.
10. Guery, J.; Favard, L.; Sirveaux, F.; Oudet, D.; Mole, D.; Walch, G. Reverse total shoulder arthroplasty. Survivorship analysis of eighty replacements followed for five to ten years. *The Journal of bone and joint surgery. American volume* **2006**, *88*, 1742–1747.
11. Cheung, E.; Willis, M.; Walker, M.; Clark, R.; Frankle, M.A. Complications in reverse total shoulder arthroplasty. *The Journal of the American Academy of Orthopaedic Surgeons* **2011**, *19*, 439–449.
12. Kwon, Y.W.; Forman, R.E.; Walker, P.S.; Zuckerman, J.D. Analysis of Reverse Total Shoulder Joint Forces and Glenoid Fixation. *Bulletin of the NYU Hospital for Joint Diseases* **2010**, *68*, 273–280.
13. Bohsali, K.I. Complications of Total Shoulder Arthroplasty. *The Journal of Bone and Joint Surgery (American)* **2006**, *88*, 2279.
14. Hong, J.; Pan, Z.; Zhewang.; Yao, M.; Chen, J.; Zhang, Y. A large-strain weft-knitted sensor fabricated by conductive UHMWPE/PANI composite yarns. *Sensors and Actuators, A: Physical* **2016**, *238*, 307–316.
15. Smith, S.; Li, B.; Buniya, A.; Lin, S.H.; Scholes, S.; Johnson, G.; Joyce, T. In vitro wear testing of a contemporary design of reverse shoulder prosthesis. *Journal of Biomechanics* **2015**, *48*, BMD1500176.
16. Matsen, F.A.; Clinton, J.; Lynch, J.; Bertelsen, A.; Richardson, M.L. Glenoid Component Failure in Total Shoulder Arthroplasty. *JBJS-A, The Journal of Bone and Joint Surgery* **2008**, pp. 885–896.
17. Nam, D.; Kepler, C.K.; Nho, S.J.; Craig, E.V.; Warren, R.F.; Wright, T.M. Observations on retrieved humeral polyethylene components from reverse total shoulder arthroplasty. *Journal of Shoulder and Elbow Surgery* **2010**, *19*, 1003–1012.
18. Terrier, A.; Reist, A.; Merlini, F.; Farron, A. Simulated joint and muscle forces in reversed and anatomic shoulder prostheses. *Bone & Joint Journal* **2008**, *90-B*, 751–756.
19. Berhouet, J.; Garaud, P.; Favard, L. Evaluation of the role of glenosphere design and humeral component retroversion in avoiding scapular notching during reverse shoulder arthroplasty. *Journal of Shoulder and Elbow Surgery* **2014**, *23*, 151–158.
20. Holness, F.B.; Price, A.D. Robotic extrusion processes for direct ink writing of 3D conductive polyaniline structures. Electroactive Polymer Actuators and Devices (EAPAD) 2016; Bar-Cohen, Y.; Vidal, F., Eds.; SPIE: Bellingham, WA, 2016; Vol. 9798, *SPIE Smart Structures and Materials + Nondestructive Evaluation and Health Monitoring*, pp. 97981G–1 – 97981G–8.
21. Blythe, A. Electrical resistivity measurements of polymer materials. *Polymer Testing* **1984**, *4*, 195–209.
22. Barra, G.M.O.; Matins, R.R.; Kafer, K.A.; Paniago, R.; Vasques, C.T.; Pires, A.T.N. Thermoplastic elastomer/polyaniline blends: Evaluation of mechanical and electromechanical properties. *Polymer Testing* **2008**, *27*, 886–892.